Current Conduction in Poly(3-Hexylthiophene) and in Poly(3-Hexylthiophene) doped [6,6]-Phenyl C61-Butyric Acid Methylester Composite Thin Film Devices

Zivayi Chiguvare[a] and Jürgen Parisi[b]

[a] University of the Witwatersrand, School of Physics (DST/CoESM, MPRI), Private Bag 3, Wits 2050, Johannesburg, South Africa

[b] University of Oldenburg, Energy and Semiconductor Research, 26111, Oldenburg, Germany

Reprint requests to Z. C.; E-mail: Zivayi.Chiguvare@wits.ac.za

Z. Naturforsch. **67a,** 589 – 600 (2012) / DOI: 10.5560/ZNA.2012-0062
Received March 26, 2012 / revised June 6, 2012 / published online September 12, 2012

Transport properties of poly(3-hexylthiophene) (P3HT), and of its blend with [6,6]-phenyl C61-butyric acid methylester (PCBM), were studied by analysing temperature dependent current–voltage characteristics of spin cast thin films sandwiched between aluminium electrodes in a metal–insulator–metal (MIM) configuration. It was found that in Al/P3HT/Al devices, the current is limited by space charge that accumulates near the hole injecting electrode due to the poor bulk transport properties of P3HT. At low temperatures and high applied electric fields the current density obeys a power law of the form $J \sim V^m$, characteristic of space charge limited current (SCLC) in the presence of exponentially distributed traps within the band gap. These traps are filled by charge that is injected by quantum mechanical tunnelling, which is adequately described by the Fowler–Nordheim (FN) theory. By calculating the majority charge carrier mobility in Al/P3HT/Al and Al/P3HT:PCBM/Al devices from the Ohmic, SCLC, and FN tunnelling fits at different temperatures, we have obtained that the charge carrier mobility in P3HT is two orders smaller than the electron mobility in the P3HT:PCBM blend at room temperature, but comparable at low temperatures. This information is important in determining the origin of open circuit voltage and short circuit current limit in solar cells that employ this blend as the active layer.

Key words: Polymer Semiconductors; Space Charge Limited Currents; Trap Filling; MIM Devices; Fowler–Nordheim Tunnelling.

PACS numbers: 72.20.Ht; 72.80.Le; 73.40.Rw; 73.40.Sx; 82.35.Cd; 85.30.De

1. Introduction

1.1. Motivation

Organic polymers are interesting materials for the fabrication of electrically conducting devices such as light emitting diodes [1], solar cells [2 – 4], and thin film field effect transistors [5] on flexible substrates. Poly(3-hexylthiophene) (P3HT) has emerged as one of the very promising materials and is currently a subject of intense research. Photovoltaic devices employing P3HT:PCBM blends as the active layer with reproducible efficiency as high as 5% at 100 $\mathrm{mW/cm^2}$, AM1.5 radiation have been achieved [6, 7]. Certified power conversion efficiency of 8.3% has been reported for bulk heterojunction organic solar cells [8], and commercial manufacture for application in consumer electronics has started.

The electron collecting electrode in polymer-fullerene heterojunction solar cells is usually aluminium, which is in contact with both P3HT and PCBM. Open circuit voltages of ~ 0.6 V and above have been achieved in these solar cells, which biases the device with electrical fields $\sim 3 \cdot 10^{-4}$ V/cm for a 200 nm thick solar cell. Current flow in these devices is therefore strongly influenced by the photo-generated voltage. The understanding of the basic physics underlying the electrical, thermal, and optical behaviour of organic polymeric materials [9], and their blends with fullerenes [10], as well as charge injection and collection dynamics across interfaces, is essential for the optimisation of devices fabricated using these materials.

In this paper, we intend to contribute towards the understanding of charge injection dynamics across

Al/P3HT and Al/PCBM interfaces and charge transport in these devices. We investigate the effect of biasing thin films of P3HT and P3HT:PCBM blends in terms of how charge is injected across the interfaces and transported through the bulk. By reverse analogy, this could assist in the understanding of charge collection from solar cells made using these materials. We report on a study of electrical and thermal properties of spin-cast films of P3HT and P3HT:PCBM blends, sandwiched between aluminium electrodes in a MIM configuration. Characteristic hole trap depths were quantified for each temperature, then used to obtain the characteristic trap energy and the total trap density in the P3HT films. We describe the complete $J(V)$ curves through a model that incorporates Richardson–Schottky (RS) thermionic, and FN tunnelling currents. Ohmic, SCLC, and FN theories were employed in obtaining the charge carrier densities and mobilities, as well as effective injection barriers. We obtained that charge carrier mobility in P3HT is more than two orders smaller than electron mobility in the P3HT:PCBM blend at room temperature.

1.2. Theory

1.2.1. Charge Injection Limited Conduction

Dark charge carrier injection depends on the potential barrier at the interface and on the temperature dependent energy of electrons incident on that barrier. The literature often presents Fowler–Nordheim (FN) straight line plots as proof of the existence of electron tunnelling as predicted by wave-mechanics. FN tunnelling is the wave-mechanical tunnelling of an electron through an exact or rounded triangular barrier (see Fig. 1). The FN model for tunnelling injection ignores

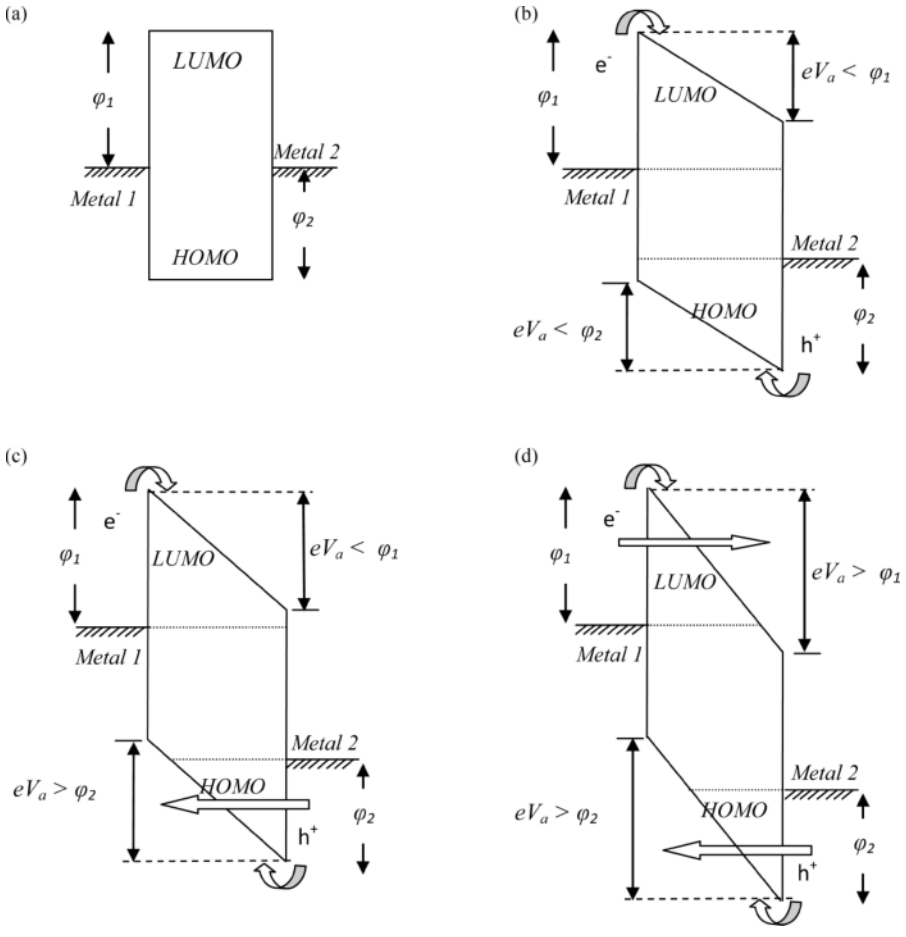

Fig. 1. (a) Typical energy diagram of a MIM device with symmetric electrodes in equilibrium; hole injection barrier φ_2 is smaller than electron injection barrier φ_1. (b) Small negative bias on *Metal 1* modifies the energy band structure, and both electrons and holes can be injected by thermionic emission over the trapezoidal barrier. The effective thickness traversed by charge carriers is the film thickness and tunnelling is negligible. (c) At intermediate applied voltages, the effective thickness for hole conduction is smaller than the device thickness, and the electrode of smaller injection barrier φ_2 injects holes significantly by FN tunnelling (hole-only device). (d) At high V_a both barriers are now smaller than qV_a, and tunnelling injection takes place from both electrodes, leading to ambipolar conduction.

image charge effects and invokes tunnelling of electrons from the metal through a triangular barrier into unbound continuum states. It predicts that the current density

$$J(F) = \frac{q^3}{16\pi^2\hbar\varphi}F^2 \exp\left[-\frac{4(2m_{\text{eff}})^{\frac{1}{2}}\cdot\varphi^{\frac{3}{2}}}{3\hbar qF}\right] \quad (1)$$

is independent of temperature. Here m_{eff} is the effective mass of the carrier inside the dielectric, q the electronic charge, $F = V_{\text{a}}/d$, where V_{a} is the applied electric field, d the film thickness, and φ the unmodified potential barrier at the metal contact/polymer interface. Barrier lowering due to an applied electric field may become comparable to the barrier height itself at higher fields, and its neglect in tunnelling considerations is problematic as are the tacit assumptions of a triangular barrier and the existence of a continuum of unbound states into which carriers can tunnel.

The essential assumption of the Richardson–Schottky (RS) model of thermionic emission is that an electron from the metal can be injected once it has acquired a thermal energy sufficient to cross the potential maximum that results from the superposition of the external and the image charge potential (see curved arrows in Fig. 1). Neither is tunnelling considered nor inelastic scattering of the hot carrier before traversing the potential maximum. The $J(F)$ characteristic is predicted as

$$J(F) = CT^2 \exp\left\{\left[-\varphi + \left(\frac{q^3F}{4\pi\varepsilon\varepsilon_0}\right)^{\frac{1}{2}}\right] \Big/ k_{\text{B}}T\right\}, \quad (2)$$

where $C = 4\pi m k_{\text{B}}{}^2 q/h^3 = 1.02173 \cdot 10^6\ \text{A/m}^2\,\text{K}^2$, k_{B} is Boltzmann's constant, T absolute temperature, ε_0 dielectric permittivity of free space, ε dielectric permittivity within the film material, and h Planck's constant. The application of the RS concept suffers from the neglect of inelastic carrier scattering inside the potential well which is of crucial importance in organic solids in which transport is an incoherent process and the mean free path is comparable to the intermolecular distance ≈ 1 nm.

Interpretation of $J(F)$ characteristics using FN and/or RS models in a mutually exclusive manner yields results of limited scope. For instance, temperature dependent current–voltage measurements on poly para phenylenevinylene (PPV) films revealed a thermally activated behaviour at low voltages [11]. The absence of this behaviour at higher voltages was attributed to field emission (FN tunnelling) at the contacts [12]. However, the theoretical FN expression was not able to quantitatively account for the experimental $J(V)$ characteristics. The large deviations were attributed to thermionic emission [13], space charge effects in the bulk of the polymer [14], and band bending effects [15]. It has been demonstrated that at low elec-

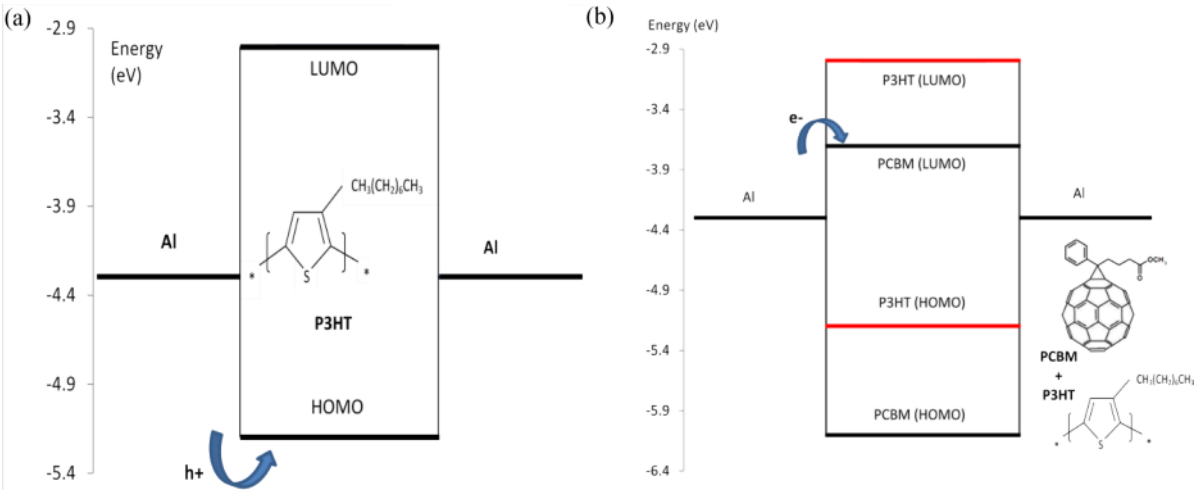

Fig. 2 (colour online). Energy levels of (a) Al/P3HT/Al hole only device and (b) Al/P3HT:PCBM/Al electron only device, with the devices in equilibrium, The insets show the chemical formula(e) of the material(s) forming the thin films under study. Arrows indicate the transport levels of the majority charge carriers when the left electrode is biased negatively.

tric fields and at room temperature the conduction of holes in PPV devices is limited by space charge effects in the bulk of the polymer and not by the charge injection from the contact [16]. At high fields however, the strong field dependence of the current together with its decreased temperature dependence both seem to argue in favour of the tunnelling model [17].

We have shown that the determination of whether conduction is contact injection limited or bulk limited is dependent upon the balance between the applied field and the temperature, where the threshold field for switch over from RS thermionic emission to FN field emission is determined by [18]

$$F = \frac{2\sqrt{2m}k_{\mathrm{B}}T\phi^{\frac{3}{2}}}{q\hbar(\phi - k_{\mathrm{B}}T)}, \tag{3}$$

when the sample is maintained at constant temperature. As T increases, the numerator increases, while the denominator decreases, hence F required for tunnelling to dominate the characteristics becomes higher. When $\varphi \leq k_{\mathrm{B}}T$, (3) is not defined, i.e. all charges have energy equal to or greater than that required to overcome the barrier, therefore only thermionic emission will occur, and the definition of quantum mechanical tunnelling is not applicable. In general, for metal/polymer interfaces it may be assumed that if RS thermionic injection dominated the injection process, then bulk conduction should be the limiting factor. If tunnelling is dominant at high F, then the contact is a limiting factor at low F only. It is possible to realize SCLC independent of injection mechanism. We show in this paper that the two charge injection mechanisms are not mutually exclusive and can occur at the same time within a device.

1.2.2. Charge Transport in the Bulk

Once charge carriers are injected, their transport through the polymer layer towards the adjacent electrode under the influence of the external electric field is determined by the conduction properties of the material itself. For low bias the number of injected carriers is smaller or comparable to the thermally generated intrinsic charge carriers, and the current–voltage characteristics can be described by Ohm's law:

$$J_{\mathrm{Ohm}} = qn\mu\frac{V_{\mathrm{a}}}{d}, \tag{4}$$

where n is the density of the majority charge carrier, and μ is the charge carrier mobility. The space charge limited current (SCLC) model [19, 20] describes charge injection into a low conductivity material, where the concentration of injected charge may exceed the intrinsic charge concentration, and space charge builds in the sample. Fits of this model provide useful material characteristics such as the trap distribution in the energy band gap, the position of the Fermi energy level, and charge carrier mobility. Investigations of low barrier devices have shown that bulk conduction in disordered, and that in undoped, conjugated polymers is also described well by the hopping transport of electrons and holes, taking into account space charge effects and traps of different depths [21].

Current density–voltage, $J(V)$, characteristics of electrode/polymer/electrode devices can often be fitted excellently by the power law $J \sim V^m$ with $m > 2$, characteristic of the filling of exponentially distributed traps [22]. Traps may originate from structural defects or due to perturbed molecules in the lattice causing charge of polarisation energy in the perturbed regions, which may also tend to lower the bottom edge of the conduction band or to raise the bottom edge of the valence band. Campbell et al. [23] have shown that the SCLC model with field independent mobility, in presence of exponentially distributed traps gives qualitatively the same results as trap free space charge limited current (TFSCLC) with a field dependent mobility of the Poole–Frenkel type [24 – 26].

The specific functional form of the SCLC $J(V)$ curve depends on the distribution of charge traps in the band gap. For traps that are exponentially distributed within the energy band gap, it is

$$N(E) = N_{\mathrm{vb}}\exp\left(-\frac{E}{E_{\mathrm{t}}}\right), \tag{5}$$

where $N(E)$ is the trap density per unit energy range at an energy level E above the valence band edge, and N_{vb} is the trap density at the valence band edge ($N_{\mathrm{vb}} = N_{\mathrm{total}}/k_{\mathrm{B}}T_{\mathrm{t}}$); E_{t} is the characteristic constant of the distribution, also often expressed as a characteristic temperature T_{t}, ($E_{\mathrm{t}} = k_{\mathrm{B}}T_{\mathrm{t}}$), where k_{B} is Boltzmann's constant. The exponential distribution of traps in a hole-only device implies a power law dependence of J on V given by [19, 20]:

$$J = q^{1-l}\mu_{\mathrm{p}}N_{\mathrm{v}}\left(\frac{2l+1}{l-1}\right)^{\frac{1}{l}}\left(\frac{l}{l+1}\frac{\varepsilon\varepsilon_0}{N_{\mathrm{total}}}\right)^{l}\frac{V^{l+1}}{d^{2l+1}}, \tag{6}$$

where μ_{p} is the charge carrier mobility of holes, N_{v} the density of states in the valence band, N_{total} the total

density of traps; $l = T_t/T$, T is the measurement temperature in K, $m = l + 1$, and $J \sim V^m$ is the power law obtained. In that case, the quasi-Fermi level, which depends on the magnitude of stored charge and hence on the applied voltage, is given by

$$E_F(V) = k_B T_t \ln\left[f(l)\frac{qN_{total}d^2}{\varepsilon\varepsilon_0 V}\right], \tag{7}$$

where

$$f(l) = \left(\frac{2l+1}{l+1}\right)^{-\frac{1}{l}} \frac{(l+1)^2}{l(2l+1)}, \tag{8}$$

and $0.5 \leq f(l) \leq 8/9$ defines the limits of validity of application of the exponential distribution model [27]. The higher extreme, $f(l) = 8/9$, corresponds to $m = 2$, i.e. all traps are filled and Child's law,

$$J_{TFSCLC} = \frac{9}{8}\varepsilon\varepsilon_0\mu\frac{V^2}{d^3}, \tag{9}$$

is obeyed, while the lower extreme, $f(l) = 0.5$, corresponds to $m = \infty$, when the slope of the $J(V)$ curves becomes vertical, and traps that are being filled are situated at a discrete level and cannot be described by an exponential distribution.

$E_F(V)$ is measured from the edge of the valence band for the hole injection, or from the conduction band edge for electron injection [5]. Upon an increase of the bias voltage, the increased positive space charge will occupy the first available trap states for holes in the bandgap, which corresponds to a shift of E_F towards the valence band edge. Further, we may rewrite (7) as

$$E_F(V) = k_B T_t\left\{\ln\left[f(l)\frac{qd^2N_{total}}{\varepsilon\varepsilon_0}\right] - \ln V\right\}. \tag{10}$$

In the SCLC regime E_F is thus linearly dependent on $(\ln V)$ [28]. The Fermi level $E_F(V)$ will coincide with the valence band edge ($E_F = 0$), only if the right-hand-side of (10) is zero. This takes place when the applied voltage V reaches a critical voltage given by

$$V = V_c = f(l)\frac{qd^2N_{total}}{\varepsilon\varepsilon_0}. \tag{11}$$

At the bias voltage V_c all the traps are filled and E_F coincides with the valence band edge energy E_{vb}. V_c and the corresponding current density J_c at this point are independent of temperature. Therefore the SCLC power law curves at different temperatures all intersect at $J = J_c$, $V = V_c$. If such a cross-over point is observed in measured $J(V)$ characteristics, one may then calculate the total trap density from (7) as

$$N_{total} = \frac{1}{f(l)}\frac{\varepsilon\varepsilon_0 V_c}{qd^2}. \tag{12}$$

A plot of E_F vs. $\ln V$ for different temperatures should then yield straight lines that converge at V_c.Thus, from the $J(V)$ characteristics obeying a power law, one may estimate the characteristic energy of the exponential distribution of traps, the trap density at E_t, at the conduction band edge, and indeed at any energy level within the band gap, the total trap density, the quasi Fermi level, as well as the activation energy.

2. Materials and Methods

The formulae of P3HT and PCBM, and energy level diagrams of the studied Al/P3HT/Al and Al/P3HT:PCBM/Al devices (under non-equilibrium conditions) are shown in the insets to Figure 2a and b, respectively. The workfunction of aluminiuml is -4.3 eV, and the highest occupied molecular orbital (HOMO) of P3HT has been estimated to range between -5.1 and -5.2 eV, from an SCLC analysis of hole only thin film devices [29], cyclic voltametry [30], and photoelectron spectroscopy [31]. The energy gap estimated from absorption spectroscopy is about 2.1 eV, therefore the lowest unoccupied molecular orbital (LUMO) is about -3.0 eV. We note therefore that the Al/P3HT/Al devices are hole only devices conducting holes through the HOMO level of P3HT, at low applied bias, since the non-equilibrium hole injection barrier is ~ 0.7 eV while the electron injection barrier is ~ 1.3 eV. The HOMO and LUMO levels of PCBM are -6.0 and -3.7 eV, respectively, The Al/P3HT:PCBM/Al devices conduct electrons through the LUMO level of PCBM and holes through HOMO of P3HT since the electron injection barrier in this case is only ~ 0.2 eV smaller than the hole injection barrier.

Glass substrates were cleaned in deionized water, acetone, toluene, and isopropanol, respectively, in a hot ultrasonic bath. The aluminium electrode in contact with the glass substrate was deposited by thermal evaporation in better than $5 \cdot 10^{-7}$ mbar vacuum. A chloroform-toluene based polymer solution (P3HT, 10 mg/ml) was then spin-coated in the nitrogen atmosphere of a glove box, O_2 – 2 ppm and H_2O –

0.01 ppm giving films of thicknesses around 140 nm. For Al/P3HT:PCBM/Al devices, a 1 : 2 polymer-fullerene blend by mass was spin coated using the same parameters as above, giving films of thicknesses around 400 nm. The aluminium top electrodes were deposited by thermal evaporation in high vacuum, better than $5 \cdot 10^{-7}$ mbar at ~ 0.2 nm/s rate. All devices were stored in nitrogen atmosphere prior to measurement.

Dark, temperature dependent, current–voltage characteristics were obtained by utilising a dc current–voltage source/monitor unit (Advantest TR 6143), as a voltage source and current monitor, with the device placed in a liquid-nitrogen-cooled cryostat at high vacuum of better than 10^{-5} mbar in all cases. The temperature range studied was from 150 to 360 K, and the temperature was allowed to stabilize for 3 minutes within ± 0.1 K before measurement was initiated. In all cases the voltage sweep was from negative to positive voltages. The thicknesses of the devices were obtained by scrapping off part of the thin polymer film, and using an atomic force microscope (Burleigh Vista-100 Scanning Probe Microscope), in the non-contact mode, to scan the formed step.

3. Results and Discussion

3.1. $J(V)$ Characteristics

Figure 3a and b show typical $J(V)$ characteristics of Al/P3HT/Al hole only devices and Al/P3HT:PCBM/Al devices, in semi logarithmic scale, in the 149 to 362 K and 194 to 360 K temperature ranges, respectively. Both devices show negligible rectification factors (less than 2 at ± 1 V). This confirms the symmetry of our devices in a MIM configuration.

The small rectification factors observed are attributed to oxidation of the first electrode during transportation of substrate from evaporation chamber to nitrogen filled glove box. Any difference observed in the electrical behaviour of the devices should therefore be primarily due to the presence of PCBM in the devices.

4. Ohmic and Space Charge Limited Currents

The curves of Figure 3a and b are re-plotted as current density–voltage plots in a double logarithmic representation in Figure 4a and b, respectively. For low temperatures below 220 K, the curves of Figure 4a have slopes that vary from 1 to 2 at low and intermediate applied electrical fields, respectively, and have slopes greater than 2 at high fields and low T. Higher temperatures did not exhibit slope equal to 2 regions, the maximum observed being 1.6 at 360 K. Curves of Figure 4a converge to a single point at high fields, while curves of Figure 4b are quasi-parallel. We investigate this difference which suggests different dominant conduction mechanisms in P3HT and

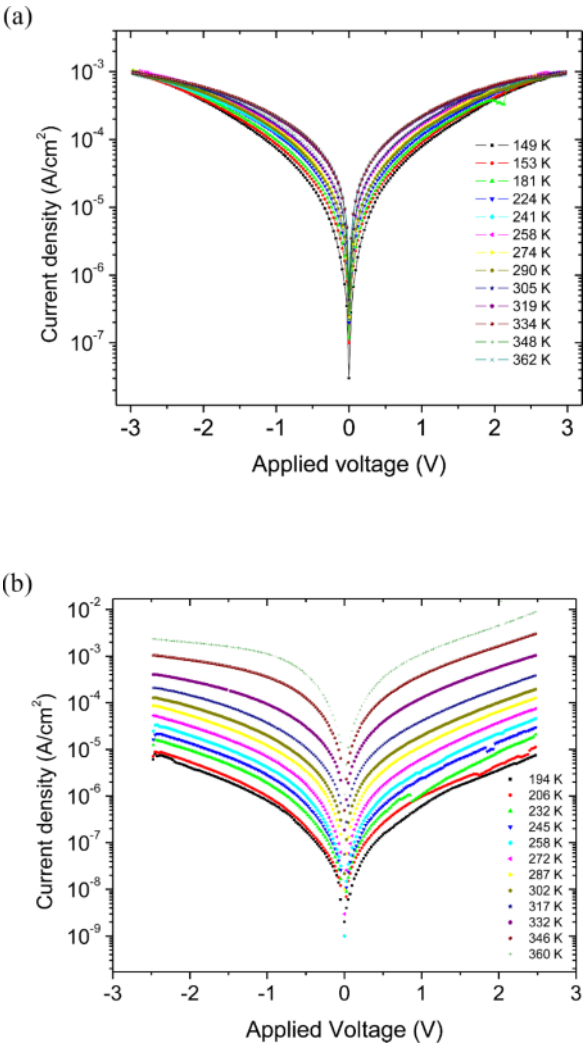

Fig. 3 (colour online). Semi-logarithmic plots of current density–voltage characteristics of (a) Al/P3HT/Al devices and (b) Al/P3HT:PCBM/Al devices at different temperatures. Curves look symmetrical at positive and negative applied electrical field, with negligible rectification factors, as expected.

P3HT:PCBM devices. We now discuss the significance of the mentioned three regions of double logarithmic $J(V)$ curves, i.e., region 1 (slope = 1), region 2 (slope ~ 2), and region 3 (slope > 2) for the studied devices.

At low bias, the current density depends linearly on the applied voltage (slope ~ 1) and Ohm's law (4) is obeyed. Thermally generated charge carriers are swept by the applied electric field and a drift current flows. In a semiconductor material with an energy gap, carriers are generated thermally by the promotion of electrons from the valence band to the conduction band. Those electrons, and holes left in the valence band, are transported via different levels, but both contribute to the total current across the device. In the case of Al/P3HT/Al devices Figure 4a, we expect extremely few thermally generated charge carriers because the electrons do not get enough thermal energy to overcome a band gap greater than 2 eV, thus slope ~ 1 region is almost not observed for low temperatures. Thermally generated charge carriers in these devices may result from unintentional p-doping of P3HT by oxygen, water, and residual impurities [32, 33]. If $1 \leq \text{slope} < 2$, charge carriers are being injected from electrodes into the material, but the material is not capable of transporting them at the same rate, i.e., some charge carriers are being stored in the material. As the applied field is increased, charge is transported at higher levels close to the transport level already populated by thermally generated carriers. These may be interpreted as traps close to the Fermi transport level of the material at that constant temperature. Once a trap is filled, it starts to contribute to the current, which then comprises of injected charge (through trap levels) and thermally generated carriers. As the temperature is increased, the density of thermally generated charge carriers increases, and hence the current is higher for the same applied voltages. The ohmic region is hence extended for a wider voltage range (see guide line at high T in Fig. 4a).

At intermediate bias, P3HT cannot transport charges at the same rate at which they are being injected, the excess injected charge due to increased applied electric field will accumulate in the material close to the injecting electrode (space charge region) once all low energy trap levels are filled up. The space charge creates a field that opposes the injection of more charges into the material and hence the current is limited by the space charge even if voltage is increased. At the trap filled limit, the $J(V)$ dependence becomes quadratic (slope = 2). We argue that this current is comparable

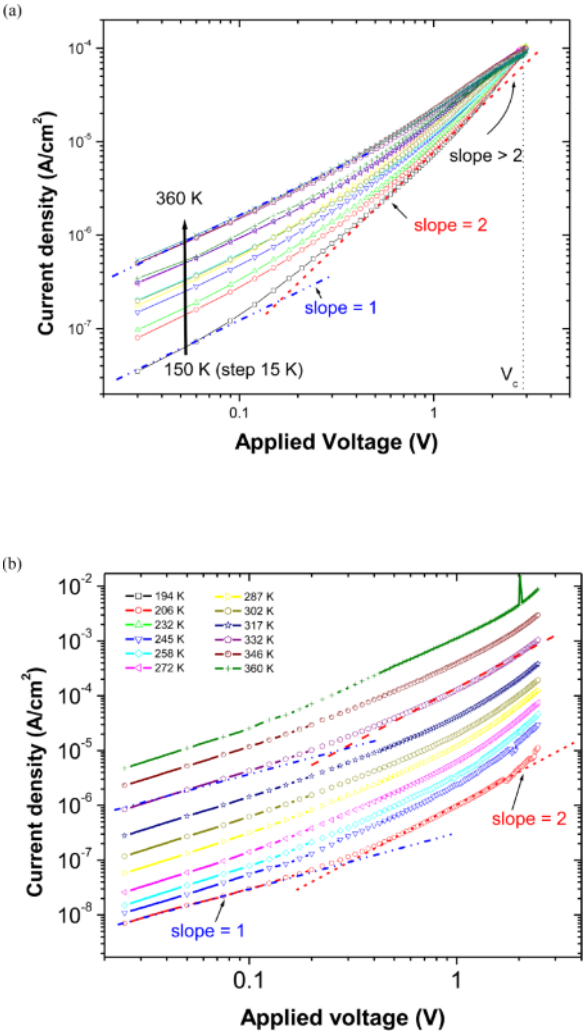

Fig. 4 (colour online). (a) Temperature dependent current density–voltage characteristics of Al/P3HT/Al devices for positive applied voltages in double logarithmic plot, showing both Ohmic and space charge limited currents (slopes, $1 \leq m \leq 2$), and filling of traps due to electric field injected charge carriers (slopes $m > 2$). All curves converge at a critical voltage V_c, where the current does not depend on temperature. (b) Double log plots of $J(V)$ characteristics of Al/P3HT:PCBM/Al devices. Regions of slopes 1 and 2 are indicated by dotted and dashed lines, respectively.

to the thermionic emission current since FN tunnelling should be negligible for such low applied bias. Figure 5 shows that we can model successfully the current as a sum of the Ohmic current (4) and trap free space charge limited current (TFSCLC) (9), thus $J_{\text{TE}} \approx J_{(\text{Ohm})} + J_{(\text{TFSCLC})}$, for the regions where $1 \leq \text{slope} \leq 2$ has been observed.

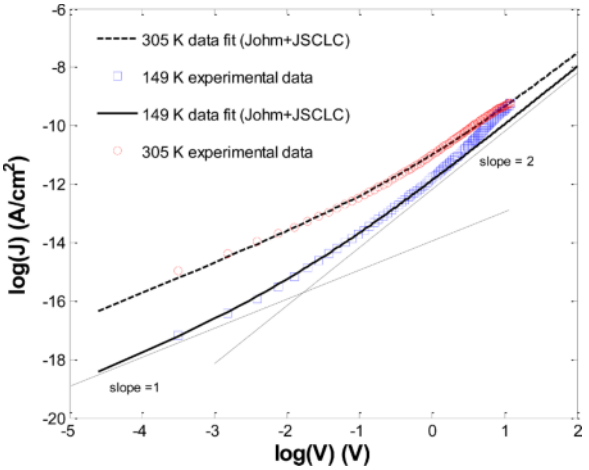

Fig. 5 (colour online). Theoretical fits of current due to thermionically injected carriers in the absence of traps $J_{TE} = J_{Ohm} + J_{TFSCLC}$ to experimental data. The fits are good where $1 \leq \text{slope} \leq 2$ has been observed in the double log $J(V)$ plot.

The slope remains equal to 2 until the energy given to the electrons by the applied electric field equals that of another trap band in the material. The accumulated space charge then suddenly rushes to occupy those traps, increasing the current significantly such that the slope is greater than 2 as indicated for low temperatures in Figure 4a. If the traps are situated at a discrete level, then an almost vertical slope is observed in the $\log J$–$\log V$ plot. Once all traps at that level/band are filled, again a space charge accumulates limiting any further injection of carriers into the material. Thereafter, the TFSCLC again flows and slope equals 2. This can repeat until all traps are filled in the material. In the studied case, however, the slope obtained in Figure 4a is superquadratic for temperatures below 240 K, hence the exponential distribution model can be used to interpret the $J(V)$ behaviour.

4.1. Traps in P3HT

The values of the slopes of the $J(V)$ curves in the double logarithmic plot for Al/P3HT/Al device were between 2.45 to 2.01 for the temperature range 149 to 224 K, with the highest slope measured for the lowest temperature. The characteristic temperature T_t obtained was 220 $\pm$20 K for the temperature range where slope $m > 2$ was obtained, corresponding to a characteristic trap parameter ($E_t = k_B T_t = 0.02$ eV). Indeed these curves converge at a voltage of 3.3 ± 0.05 V, and this was considered as V_c, which we substituted in (12) to obtain a total hole trap density within the band gap of between $5.1 \cdot 10^{16}$ cm^{-3} and $9.1 \cdot 10^{16}$ cm^{-3} as evaluated for the two extremes of validity of the exponential trap distribution described in Section 1.2.2. We note that for each particular temperature the slope obtained will define the value of $f(l)$ according to (12), and hence N_{total} is available for conduction at that temperature. The obtained characteristic trap energy suggests that at about 220 K it should be expected that the number of traps filled is $1/e$ of the total available. Above this temperature, therefore, the conduction should not be trap limited, since practically all traps are filled.

Once traps are filled, they start to contribute to current conduction, i.e., electrons with energies below or equal to the trap energy level behave like free electrons. Hence trap filling is equivalent to increasing the density of charge carriers in the device. If the mobility in the material is low, and the injection mechanism is efficient, space charge limited currents may be observed. If however the charge injection mechanism is inefficient, Ohm's law will dominate the characteristic.

Charge injection takes place through quantum mechanical tunnelling and thermionic emission. Tunnelling is dominant at low temperatures and high electric fields while thermionic emission is dominant at high temperatures. Both injection mechanisms can fill-up traps situated at the same levels independent of applied electric field and temperature. When all the existing traps are filled, the current that flows through a device is then independent of temperature and this can manifest as a single point where the J–V curves for different temperatures intersect. This is clearly evident in Figure 4a, where all the curves converge at a point (J_c, V_c).

4.2. Space Charge Limited Currents in P3HT:PCBM Blend

In Figure 4b the curves exhibit slopes 1 and 2 as indicated by the guide lines. We note that for all the curves there is a small region at very high applied fields where the slope is greater than 2. The current conduction is therefore Ohmic at low applied voltages V_a with slope ~ 1, and space charge limited with slopes ~ 2 at higher V_a. By equating Ohm's law (4) to Child's law (9) at the point where the straight lines describing these laws intersect (V_x, J_x), and assuming field independent electron mobility, we estimated the majority charge

carrier mobility in the Al/P3HT:PCBM/Al devices at different temperatures to be between $3.45 \cdot 10^{-6}$ and $5.76 \cdot 10^{-5}$ cm^2/Vs for the 194 K to 302 K temperature range. This method could not be used for Al/P3HT/Al devices at lower temperatures because the slope equal to 1 region could not be observed, suggesting space charge limitation even at low voltages. We note also that the curves of Figure 4b are quasi parallel as opposed to the convergent nature observed in Figure 4a. Therefore, we cannot assume an exponential distribution of traps in P3HT:PCBM material blends.

Electron transport in a trap free molecularly doped polymer optimised for electron transport, such as our Al/P3HT:PCBM/Al devices, involves a field driven chain of redox reactions in which the carrier hops from a neutral molecule and its radical cation derivative. The electron transport process is triggered by an initial charge transfer in which a neutral molecule, P3HT, is energetically favoured to donate an electron either to an adjacent metal contact or to the LUMO of PCBM. If the neutral transport molecule has an electron affinity higher than any competing species present, then the latter is independent of their concentration, cannot act as traps; thus they are invisible to transiting electrons. A complementary situation can be described in terms of relative ionisation potentials for hole transporting systems. These layers are therefore trap free insulators with finite unipolar mobility which means that while there are no intrinsic free carriers, an extrinsic carrier once injected, will, under the influence of an electric field, traverse the sample bulk without being locally neutralised or immobilised.

We examined the nature of charge injection for the devices in a bid to understand the origins of the differences in the nature of the observed behaviours (Section 5). It was then possible to obtain the mobility and charge carrier densities in the whole temperature range studied, and therefore to compare and make conclusions on the conduction mechanisms in Al/P3HT/Al and Al/P3HT:PCBM/Al devices.

5. Fowler–Nordheim Tunnelling Currents

We argue that the trap filling region observed in Figure 4a and discussed in Section 1.2.1 above coincides with the FN tunnelling regime indicated in FN plots of Figure 6a, i.e., where the curves can be approximated to straight lines at high applied electric fields (see inset). We note that the thermionic injection current ($J_{\mathrm{TE}} \approx J_{\mathrm{Ohm}} + J_{\mathrm{TFSCLC}}$) at low applied bias gives a curve of positive slope in an FN plot, while the FN tunnelling current gives a straight line of negative slope. In a single device, all two effects are present and the total current can therefore be calculated by

$$J(V_{\mathrm{a}}) = J_{\mathrm{TE}} + J_{\mathrm{FN}}\,. \tag{13}$$

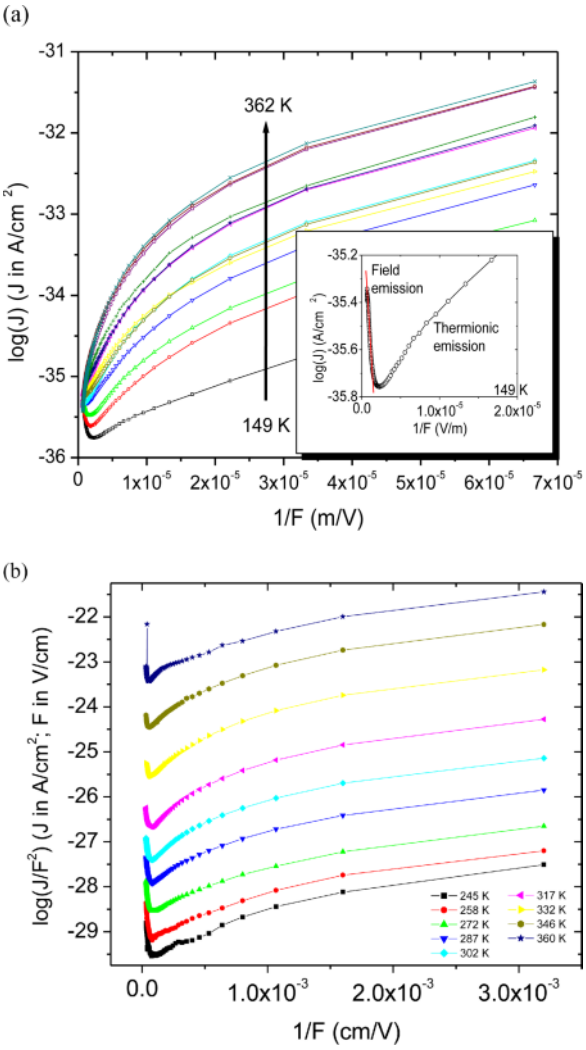

Fig. 6 (colour online). (a) Fowler–Nordheim curves showing the quantum mechanical tunnelling, space charge, and thermionic emission regimes for Al/P3HT/Al devices at different temperatures. At high temperatures only thermionic emission regime is observed. The inset shows the straight line approximation at high applied electrical fields for $T = 149$ K. (b) FN plots for Al/P3HT:PCBM/Al devices are showing that even at high temperatures the tunnelling regime is still observed. The curves look parallel to one another.

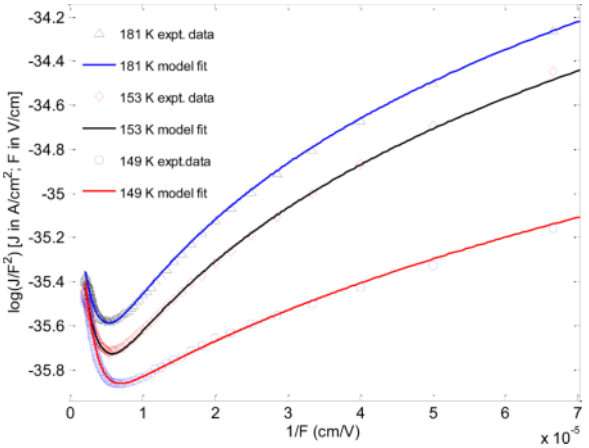

Fig. 7 (colour online). FN curves at different temperatures showing data fits of a model that considers the total current as the sum of Ohmic, TFSCLC, and FN tunnelling currents.

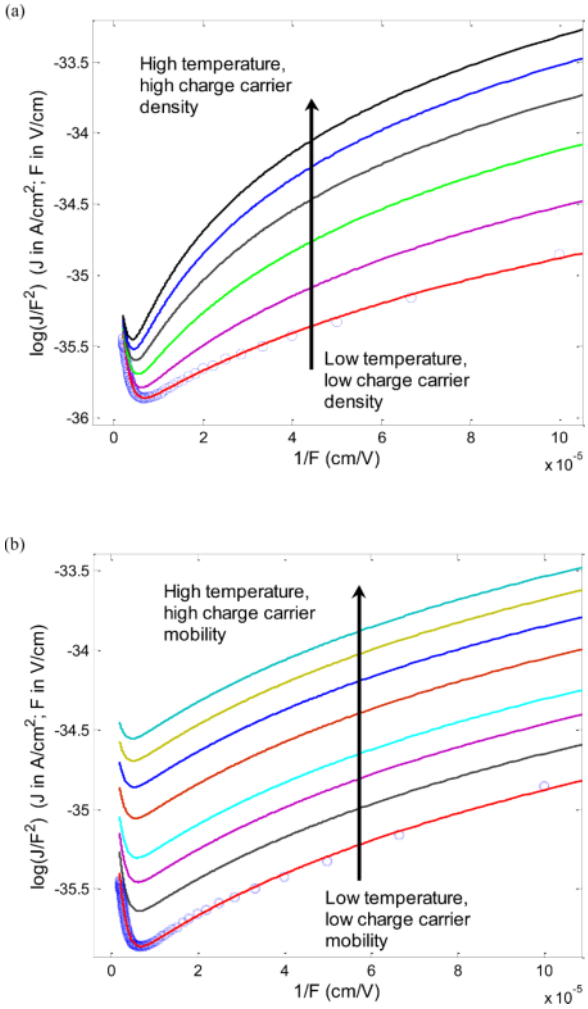

Fig. 8 (colour online). (a) FN plots showing the effect of increasing charge carrier density due to increase in temperature. The tunnelling regime becomes smaller as the temperature increases. Space charge regime dominates conductivity. Notice how the curves come closer together with a uniform increase of the density from $8.0 \cdot 10^{17}$ to $5.0 \cdot 10^{18}$ /cm^3. (b) FN plots showing the effect of increasing charge carrier mobility due to increase in temperature. The curves are quasi-parallel to each other.

Equation (13) gives good data fits to single carrier $J(V)$ experimental data as shown in Figure 7 for Al/P3HT/Al devices. The fitting hole mobilities for the three curves considered here are 3.88, 4.00 and $4.01 \cdot 10^{-7}$ cm^2/Vs, and charge carrier densities are $8.7 \cdot 10^{17}$ cm^{-3}, $1.8 \cdot 10^{18}$ cm^{-3}, and $3.9 \cdot 10^{18}$ cm^{-3}, respectively, from low to high temperature. The effective hole injection barrier in this case is obtained as 0.88 eV for $T = 149$ K. We note that these hole densities are higher than the hole trap densities calculated in Section 4.1 above, indicating that both the trap assisted hole tunnelling and thermionically emitted carriers contribute to the electrical conduction in Al/P3HT/Al devices.

We simulated the $J(V)$ characteristics of our devices by using (13) and an in-house developed Matlab programme. For example by considering all factors constant and varying only the density of charge carriers, we obtained the curves in Figure 8a. If only the charge carrier mobility is varied then we obtain the curves of Figure 8b. Experimental data for AlP3HT/Al device at 149 K is included with its theoretical fit for comparison purposes in both cases. The curves obtained in Figure 8a have a similar nature to the ones obtained experimentally for the Al/P3HT/Al device (see Fig. 6a). We can therefore infer that the temperature dependent $J(V)$ characteristics of Al/P3HT/Al devices in a FN plot show that the density of majority charge carriers in the bulk increases with increase in temperature. The charge carrier mobility of holes in this device is of the order $\sim 4.0 \cdot 10^{-7}$ cm^2/Vs for the 149 to 224 K temperature range studied. The charge carrier mobility increases only slightly, up to $\sim 4.8 \cdot 10^{-7}$ cm^2/Vs for all temperatures up to 362 K. The obtained mobilities are one to two orders smaller than the ones obtained by Choullis et al. [34] from time-of-flight photocurrent experiments possibly due to the rigorous purification procedures to which they subjected their P3HT. It is

known for instance that oxygen and residual impurities can result in p-doping of polymers [32], and differences in nanomorphology of the blend [8] can significantly influence the result.

On the other hand, the $J(V)$ characteristics of the Al/P3HT:PCBM/Al device show thermal activation behaviour, where the mobility is the main variable with temperature. We note that the curves are quasi parallel and similar to the ones obtained where mobility is the main variable (cf. Fig. 6b and 8b). Electron mobility is obtained from the fits to curves of Figure 6b to vary by three orders, i.e., from $4.5 \cdot 10^{-7}$ to $2 \cdot 10^{-4}$ cm^2/Vs in the temperature range 194 to 360 K. We conclude that the charge carrier mobilities for Al/P3HT/Al devices are comparable to those of Al/P3HT:PCBM/Al devices at low temperatures, but electron mobility becomes significantly higher than hole mobility at room temperatures and above. Low charge carrier mobilities were also observed for pristine PPV and for P3HT, and our observation of higher electron mobilities in the blend is consistent with Brabec et al. [35]. The obtained values are comparable to those obtained by Shrotriya et al. [36] for their P3HT:PCBM blends where electron mobility was also found to be slightly higher than hole mobility. Electron and hole mobilities in P3HT were found to be of the same order by Choulis et al. [34].

6. Conclusions

It has been shown that the trap assisted tunnelling current in Al/P3HT/Al devices can be successfully modelled as the sum of RS thermionic and FN tunnelling currents. Further we established that the transport level in a P3HT:PCBM blend is the LUMO of PCBM which forms an Ohmic contact with aluminium. We have shown that the hole carrier mobility through HOMO of P3HT is more than two orders smaller than electron mobility through LUMO of PCBM in a P3HT:PCBM blend thin film device. Such differences in mobility mean that electrons can travel faster than holes in the blend. This information is important for the design of photovoltaic devices based on such polymer-fullerene blends.

Acknowledgements

Z. C. is grateful for the sponsorship offered by the GTZ and DAAD. All experiments were conducted at the EHF University of Oldenburg.

[1] J. Shina, Organic Light Emitting Devices, A Survey, Springer Verlag, New York 2004.
[2] C. J. Brabec, V. Dyakonov, J. Parisi, and N. S. Sariciftci, Organic Photovoltaics: Concepts and Realization, Springer Series in Material Science, 60, Springer Verlag, Berlin, Heidelberg 2003.
[3] T. Markvart and L. Castaner, Practical Handbook of Photovoltaics, Fundamentals and Applications, Elsevier Science Limited, Oxford 2003.
[4] C. Deibel and V. Dyakonov, Rep. Prog. Phys. **73**, 096401 (2010).
[5] C. D. Dimitrakopoulos and J. D. Mascaro, IBM J. Res. Dev. **45**, 11 (2001).
[6] G. Dennler, M. C. Scharber, and C. J. Brabec, Adv. Mater. **21**, 1323 (2009).
[7] W. Ma, C. Yang, X. Gong, K. Lee, and A. J. Heegar, Adv. Funct. Mater. **15**, 1617 (2005).
[8] M. A. Green, K. Emery, Y. Hishikawa, and W. Warta, Prog. Photovolt. **19**, 84 (2011).
[9] Y. Shen, M. W. Klein, D. B. Jacobs, J. C. Scott, and G. G. Malliaras, Phys. Rev. Lett. **86**, 3867 (2001).
[10] M. Campoy-Quiles, T. Ferenczi, T. Agostinelli, P. G. Etchegoin, Y. Kim, T. D. Anthopoulos, P. N. Stavrinou, D. D. C. Bradley, and J. Nelson, Nat. Mat. **7**, 158 (2008).
[11] R. N. Marks, D. D. C. Bradley, R. W. Jackson, P. L. Burn, and A. B. Holmes, Synth. Met. **57**, 4128 (1993).
[12] J. D. Parker, J. Appl. Phys. **75**, 1656 (1994).
[13] H. Vestweber, J. Pommerrehne, R. Sander, R. F. Mahrt, A. Greiner, W. Heity and J. Baessler, Synth. Met. **68**, 263 (1995).
[14] P. E. Burrows and S. R. Forrest, Appl. Phys. Lett. **64**, 2285 (1993).
[15] E. Ettedgui, H. Razafitrimo, Y. Gao, and B. R. Hsieh, Appl. Phys. Lett. **67**, 2705 (1995).
[16] P. W. M. Blom, M. J. M. de Jong, and J. J. M. Vlegaar, Appl. Phys. Lett. **68**, 3308 (1996).
[17] P. W. M. Blom, M. J. M. de Jong, and M. G. van Munster, Phys. Rev. B **55**, R656 (1997).
[18] Z. Chiguvare, J. Parisi, and V. Dyakonov, J. Appl. Phys. **94**, 2440 (2003).
[19] K. C. Kao and W. Hwang, Electrical Transport in Solids, with Particular Reference to Organic Semiconductors, International Series in the Science of the Solid State, Vol. 14, Pergamon Press, Oxford 1981.
[20] M. A. Lambert and P. Mark, Current Injection in Solids, Academic, New York 1970.
[21] V. I. Arkhipov, P. Heremans, E. V. Emilianova, G. J. Adriaenssens, and H. Bässler, Appl. Phys. Lett. **82**, 3245 (2003).

[22] V. Kumar, S. C. Jain, A. K. Kapoor, W. Geens, T. Aernauts, J. Poortmans, and R. Mertens, J. Appl. Phys. **92**, 7325 (2002).
[23] A. J. Campbell, M. S. Weaver, D. G. Lidzey, and D. D. C. Bradley, J. Appl. Phys. **84**, 6737 (1998).
[24] W. P. Blom and M. C. J. M. Vissenberg, Mater. Sci. Eng. R**27**, 53 (2000).
[25] W. Brütting, S. Berleb, and A. G. Mückl, Org. Electron. **2**, 1 (2001).
[26] S. C. Jain, W. Geens, A. Mehra, V. Kumar, T. Aernouts, J. Poortmans, R. Mertens, and W. Willander, J. Appl. Phys. **89**, 3804 (2001).
[27] Z. Chiguvare, and V. Dyakonov, Phys. Rev. B. **70**, 235207 (2004).
[28] S. J. Tans, R. G. Miedema, L. J. Geerligs, C. Dekker, J. Wu, D. Neher, and D. Wegner, Nanotechnol. **14**, 1043 (2003).
[29] D. Chirvase, Z. Chiguvare, M. Knipper, J. Parisi, V. Dyakonov, J. C. Hummelen, Synt. Met. **138**, 299 (2003).
[30] R. Valaski, L. M. Moreira, L. Micaroni, and I. A. Hümmelgen, J. Appl. Phys. **92**, 2035 (2002).
[31] M. Onoda, K. Tada, A. A. Zakhidov, and K. Yoshino, Thin Solid Films **331**, 76 (1998).
[32] S. Karg, M. Meir, and W. Riess, J. Appl. Phys. **82**, 1951 (1997).
[33] Z. Chiguvare, J. Parisi, and V. Dyakonov, Z. Naturforsch. **62a**, 609 (2007).
[34] S. A. Choulis, Y. Kim, J. Nelson, D. D. C. Bradley, M. Giles, M. Shkunov, and I. McCulloch, Appl. Phys. Lett. **85**, 3890 (2004).
[35] C. Brabec, V. Dyakonov, and U. Scherf, Organic Photovoltaics, Materials, Device Physics and Manufacturing Technologies, Wiley VCH Verlag, Weinheim, 2008, p. 282 – 295, ISBN 978-3-527-31675-5.
[36] V. Shrotriya, Y. Yao, G. Li, and Y. Yang, Appl. Phys. Lett. **89**, 063505 (2006).